Research Square

Preprints are preliminary reports that have not undergone peer review.
They should not be considered conclusive, used to inform clinical practice,
or referenced by the media as validated information.

Neuroimmune and Sex-Associated Behavioral Alterations in a Hippocampal α-Synuclein Mouse Model of Lewy Body Dementia

Jung Ha Byun
University of Georgia
Brice Hudson
University of Georgia
Declan Gresham
University of Georgia
Adetutu Adebowale
University of Georgia
Jina Lim
University of Georgia
Jaegwon Chung
University of Georgia
Woo-Hyun Cho
Rutgers-Robert Wood Johnson Medical School
Yoon-Seong Kim
Rutgers-Robert Wood Johnson Medical School
Nikolay Filipov
University of Georgia
Jae-Kyung Lee
jamlee@uga.edu

University of Georgia

Article

Keywords: Neurodegeneration, Parkinson's Disease Dementia, Dementia with Lewy Bodies, glia, monocyte, immune response, immune cell infiltration, CX3CR1, CCR2

Posted Date: November 11th, 2026

DOI: https://doi.org/10.21203/rs.3.rs-11434752/v1

License: This work is licensed under a Creative Commons Attribution 4.0 International License.
Read Full License

Additional Declarations: Competing interest reported. J.K.L. serves as a scientific advisor for Neuronity Therapeutics, Inc. All other authors declare no competing interests.

Neuroimmune and Sex-Associated Behavioral Alterations in a Hippocampal α-Synuclein Mouse Model of Lewy Body Dementia

Jung Ha Byun[1,2†], Brice Hudson[1,2†], Declan Gresham[1,3], Adetutu Adebowale[1,3], Jina Lim[1], Jaegwon Chung[1], Woo-Hyun Cho[5], Yoon-Seong Kim[5], Nikolay Filipov[1,2,3,4]*, Jae-Kyung Lee[1,2,3]*

[1]Department of Physiology and Pharmacology, University of Georgia, Athens, GA 30602, USA

[2]Neuroscience Program, University of Georgia, Athens, GA 30602, USA

[3]Integrative Physiology and Pharmacology Program, University of Georgia, Athens, GA 30602, USA

[4]Interdisciplinary Toxicology Program, University of Georgia, Athens, GA 30602, USA

[5]RWJMS Institute for Neurological Therapeutics, Rutgers-Robert Wood Johnson Medical School, Piscataway, New Jersey 08854, USA

[†]J.H.B. and B.H. contributed equally to this work.

*Corresponding author: Dr. Jae-Kyung Lee (jamlee@uga.edu) and Dr. Nikolay Filipov (filipov@uga.edu)

Abstract

Lewy body dementias (LBDs) are characterized by α-synuclein (α-syn) aggregation, cognitive impairment, and neuropsychiatric symptoms. Associated neuroimmune and behavioral changes remain incompletely characterized in experimental models across sexes and time points. Male and female mice received hippocampal injections of α-syn preformed fibrils (PFFs) or monomers. Outcomes were assessed at 1 and 3 months post-injection (MPI). PFF-injected mice developed proteinase K-resistant phosphorylated α-syn pathology in hippocampal subfields and entorhinal cortex. Absence in α-syn-knockout mice at 5MPI supported dependence on endogenous α-syn. Pathology was accompanied by neuronal degeneration and increased glial immunoreactivity, particularly in the dentate gyrus, alongside increased $CCR2^{+}$ area consistent with monocyte recruitment. Cognitive impairments varied by task and time point, with greater anxiety-like behavior at 3 MPI. Peripheral immune profiles varied primarily by sex and time. These findings characterize neuroimmune changes and selective nonmotor behavioral abnormalities, supporting this hippocampal PFF model as a valuable tool for investigating LBD mechanisms.

Keywords

Neurodegeneration, Parkinson's Disease Dementia, Dementia with Lewy Bodies, glia, monocyte, immune response, immune cell infiltration, CX3CR1, CCR2

Introduction

Lewy body dementias (LBDs) encompass dementia with Lewy bodies (DLB) and Parkinson's disease dementia (PDD), two neurodegenerative disorders characterized by intraneuronal inclusions containing aggregated α-synuclein (α-syn) [1, 2]. DLB is considered one of the most common neurodegenerative dementias after Alzheimer's disease (AD), although prevalence estimates vary considerably across populations and diagnostic settings [3, 4]. DLB and PDD share many clinical and neuropathological features but are distinguished clinically by the timing of dementia relative to the onset of parkinsonism [2]. Cognitive impairment in DLB typically involves attention, executive function, and visuospatial processing and may be accompanied by cognitive fluctuations, visual hallucinations, rapid eye movement (REM) sleep behavior disorder, parkinsonism, and neuropsychiatric symptoms [1, 2]. Because these features can overlap with those of AD and other neurodegenerative disorders, accurate clinical diagnosis remains challenging. In LBD, Lewy pathology extends beyond the brainstem into limbic and neocortical regions, including the entorhinal cortex, hippocampus, and frontal cortex [2, 5]. Notably, α-syn pathology within the hippocampus and associated limbic regions has been linked to memory impairment, supporting the relevance of these regions to LBD-related cognitive dysfunction [6, 7].

Biological sex may influence the prevalence, clinical presentation, and neuropathological features of LBD, but the available evidence remains inconsistent [8]. Although several studies have reported a higher prevalence or diagnostic frequency of DLB in men, others have identified a more balanced sex distribution or slight female predominance [3, 4, 8]. Recent studies have also reported differences between women and men in the onset and course of symptoms, as well as in the relationship between brain pathology and clinical presentation. [9-13]. These differences may

extend to neuropsychiatric symptoms. For example, one study reported more frequent disinhibition in females two years before DLB diagnosis, although the number of affected participants was small [12]. Anxiety and depression are also common across synucleinopathies, with a meta-analysis reporting higher prevalence and greater severity in females than in males [14]. However, these findings vary across studies, possibly because of differences in diagnostic practices and coexisting AD pathology. Moreover, biological sex remains insufficiently examined in experimental synucleinopathy models.

Intracranial injection of α-syn preformed fibrils (PFFs) is commonly used to induce Lewy pathology in rodents. Following neuronal uptake, exogenous PFFs recruit endogenous α-syn and promote its aggregation into phosphorylated and proteinase K-resistant inclusions [15-17]. Many PFF studies have used intrastriatal injection to model the nigrostriatal pathology and motor features of Parkinson's disease [18, 19]. In contrast, injection into the hippocampus and adjacent forebrain regions induces α-syn pathology within hippocampal-entorhinal circuits and allows investigation of cognitive and neuropsychiatric features relevant to LBD [20, 21]. Previous hippocampal or forebrain PFF studies have reported α-syn propagation, glial responses, neuronal degeneration, and cognitive dysfunction. However, few studies have examined these neuropathological and behavioral outcomes alongside monocyte infiltration into the central nervous system (CNS) and peripheral immune profiles or evaluated how these features vary by sex and time after injection [20-22]. Therefore, comprehensive characterization of their neuropathological, immunological, and nonmotor behavioral outcomes not limited to cognition is needed to better understand the relationship among hippocampal α-syn pathology, immune responses, and nonmotor behavioral dysfunction.

Peripheral immune cells may also contribute to α-syn-associated neuroinflammation. Experimental α-syn models have demonstrated recruitment of circulating monocytes and other leukocytes to the CNS, as well as changes in immune cell profiles within peripheral lymphoid organs [18, 23, 24]. Nevertheless, peripheral immune involvement has been studied less extensively in models targeting LBD-relevant hippocampal circuits. The *Cx3cr1*^{GFP}/*Ccr2*^{RFP} reporter system enables visualization of resident and recruited myeloid populations through their differential expression of CX3CR1 and CCR2 [25]. This model therefore allows us to examine where CCR2^{+} cells accumulate and whether they localize to areas enriched with resident microglia (CX3CR1^{+}) that are affected by α-syn pathology.

In the present study, we characterized the neuropathological, immunological, and behavioral features of a hippocampal α-syn PFF mouse model at 1- and 3-months post-injection (MPI). We assessed the regional distribution of α-syn pathology and its dependence on endogenous α-syn, together with neuronal degeneration, glial responses, and CCR2^{+} cell infiltration. We also evaluated spatial and recognition memory, anxiety-related behaviors, and peripheral immune cell profiles. These analyses aimed to determine how well the model reproduces neuropathological, immunological, and nonmotor features relevant to LBD and to characterize sex- and time-associated variation within the model.

Results

Hippocampal injection of α-synuclein PFFs induces α-syn pathology in hippocampal subfields and the lateral entorhinal cortex

We aimed to induce α-syn pathology primarily in the hippocampus and associated limbic regions affected in LBD and sought to validate whether hippocampal injection of α-synuclein preformed fibrils (PFFs) induces pathological α-syn aggregation in brain regions relevant to Lewy body diseases. To address this, we unilaterally injected either α-syn monomers or PFFs into the mouse hippocampus. pSer129 was used as a marker of pathological α-syn accumulation in the hippocampal subfields, including the dentate gyrus (DG), CA1, and CA3, as well as in the lateral entorhinal cortex (LEnt) and amygdala (Amyg), at 1 and 3MPI (**Fig. 1a**). Brain sections were pretreated with proteinase K (PK) to detect insoluble, PK-resistant pSer129^{+} α-syn aggregates. Compared with monomer-injected controls, PFF-injected mice exhibited robust PK-resistant pSer129^{+} α-syn pathology in the DG (Mono vs. 1MPI, $P < 0.0001$; Mono vs. 3MPI, $P < 0.0001$), CA1 (Mono vs. 1MPI, $P = 0.0276$; Mono vs. 3MPI, $P = 0.0003$), CA3 (Mono vs. 1MPI, $P < 0.0001$; Mono vs. 3MPI, $P < 0.0001$) and LEnt (Mono vs. 1MPI, $P = 0.0061$; Mono vs. 3MPI, $P = 0.0455$), at both time points (**Fig. 1b, c**). In contrast, little to no PK-resistant pSer129^{+} α-syn pathology was detected in the amygdala or in the corresponding regions of the contralateral hemisphere (**Fig. 1b, Supplementary Fig. 1b**). The injection site was confirmed, and α-syn pathology was detected as early as 16 days post-injection (DPI) (**Supplementary Fig. 1a**).

To examine whether PFF-induced α-syn pathology depends on endogenous α-syn expression, α-syn PFFs were injected into the hippocampus of wild-type (WT) and α-syn knockout (Syn KO) mice. At 5MPI, robust PK-resistant pSer129^{+} α-syn pathology was detected in WT mice, whereas no detectable pathology was observed in Syn KO mice (**Fig. 1d**). Together, these findings

demonstrate that hippocampal PFF injection induces endogenous α-syn aggregation in the hippocampus and LEnt and that the formation of persistent PK-resistant pSer129$^+$ α-syn pathology requires endogenous α-syn expression.

The pathological α-synuclein drives neuroinflammation and neuronal degeneration

Microgliosis and astrogliosis are well-established neuropathological features that frequently accompany α-syn pathology in experimental models and human synucleinopathies [19, 26, 27]. However, evidence of glial responses in the hippocampus, a brain region closely associated with cognitive impairment in LBD, remains limited. We therefore investigated whether PFF-induced α-syn pathology is accompanied by glial changes in affected hippocampal regions and other limbic regions. We performed immunofluorescence staining for Iba-1 and GFAP in WT mice to assess microglial and astrocytic responses, respectively. Unilateral injection of α-syn PFFs significantly increased the total Iba-1$^+$ area in the DG (Mono vs. 1MPI, P = 0.0001; Mono vs. 3MPI, P = 0.0407) and CA3 (Mono vs. 1MPI, P = 0.0012; Mono vs. 3MPI, P = 0.0112). By comparison, the total GFAP$^+$ area was significantly increased in the DG only at 1MPI compared with both the monomer-injected control group (P = 0.0128) and the 3MPI PFF group (P = 0.0246) (**Fig. 2a-c**).

We next examined whether PFF-induced α-syn pathology was accompanied by neuronal degeneration or loss using immunofluorescence staining for NeuN and Fluoro-Jade C (FJC), respectively. Quantification revealed a significant reduction in the percentage of the ROI occupied by NeuN$^+$ staining in the DG at 1MPI (P = 0.0009), suggesting a loss of neuronal abundance (**Fig. 2d, e**). Consistent with this observation, the percentage of the ROI occupied by FJC$^+$ staining was significantly increased in the DG at 1MPI (P = 0.0037), indicating ongoing neuronal degeneration

(**Fig. 2d, f**). Together, these findings show that hippocampal α-syn pathology is accompanied by increased glial immunoreactivity and neuronal degeneration, particularly in the DG.

CCR2$^+$ monocyte infiltration into the CNS accompanies α-syn pathology

Previous studies have reported the infiltration of peripheral monocytes into the central nervous system (CNS) in mouse models of Parkinson's Disease (PD) [23, 24]. To investigate whether α-syn PFFs promote the recruitment of CCR2$^+$ monocytes into the hippocampus, and to distinguish these cells from resident microglia (CX3CR1$^+$), we bilaterally injected α-syn monomers or PFFs into the hippocampus of the *Cx3cr1*^{GFP}/*Ccr2*^{RFP} mice (**Fig. 3a**). Immunofluorescence staining for pSer129 and NeuN was performed, and the distributions of CX3CR1$^+$ and CCR2$^+$ cells were evaluated in regions exhibiting α-syn pathology at 1MPI. (**Fig. 3b, f**). Quantification of the immunoreactive area revealed a significant increase in the total CCR2$^+$ area per ROI in the DG ($P = 0.0418$) and CA1 ($P = 0.0271$) of PFF-injected mice compared with monomer-injected controls (**Fig. 3c**). These regions also exhibited significant increases in the total CX3CR1$^+$ area. More broadly, the CX3CR1$^+$ area was significantly increased in all hippocampal subfields examined, including DG ($P = 0.0025$), CA1 ($P < 0.0001$), and CA3 ($P = 0.0003$) (**Fig. 3d**). Consistent with the findings in unilaterally injected WT mice, PFF-injected *Cx3cr1*^{GFP}/*Ccr2*^{RFP} mice exhibited a significantly increased pSer129$^+$ α-syn pathology throughout the hippocampal subfields and the LEnt ($P < 0.0001$) (**Fig. 3e**). Among the markers examined, sex-stratified analysis revealed a significantly greater GFAP$^+$ total area in CA1 in females than in males in both the monomer-injected ($P = 0.005$) and PFF-injected groups ($P = 0.005$). GFAP$^+$ total area was also significantly greater in the PFF-injected group in each sex group (**Supplementary Fig. 2d**). Notably, CX3CR1 and CCR2 signals were colocalized in a subset of cells within the DG,

where α-syn pathology was most abundant, supporting the infiltration of $CCR2^+$ monocytes into the hippocampus (**Fig. 3b**). A subset of these cells also expressed $CX3CR1^+$. These $CX3CR1^+/CCR2^+$ cells may represent infiltrating $CCR2^+$ inflammatory monocytes undergoing phenotypic adaptation toward a CNS macrophage-like state [28]. In addition, the percentage of the ROI occupied by $NeuN^+$ staining was significantly reduced in the DG of PFF-injected mice (P = 0.0148), supporting neuronal loss in this independent *Cx3cr1*^{GFP}/*Ccr2*^{RFP} mouse cohort (**Fig. 3g**).

The α-synuclein PFF-injected mice display selective impairments in spatial memory and novelty recognition

Cognitive impairment is a common clinical feature of Lewy body diseases [6, 7]. Because the hippocampus exhibited substantial α-syn pathology in our model, we evaluated hippocampus-dependent cognitive functions, including spatial learning, spatial memory, and novelty recognition, at 1 and 3MPI. In the Barnes maze, the distance traveled to locate the target hole during acquisition did not differ significantly between the PFF- and the monomer-injected groups at 1MPI, suggesting that α-syn pathology did not impair spatial learning acquisition under these experimental conditions (**Fig. 4a**). On acquisition day 4 at 3MPI, females traveled a greater distance to the target hole than males across treatment groups (main effect of sex: F (1, 18) = 20.946, $P < 0.001$). PFF-injected mice traveled farther than monomer-injected controls, although the main effect of treatment did not reach statistical significance (P = 0.064). No significant sex x treatment interaction was detected (P = 0.319). No significant treatment effects were detected on the other acquisition days (**Fig. 4b**). During the probe trial, PFF-injected mice made significantly fewer investigations of the target hole than monomer-injected controls at 1MPI (P = 0.0306), whereas no significant difference was observed at 3MPI (**Fig. 4c, d**). At 1MPI, DG $pSer129^+$ α-

191 syn area was also negatively correlated with the number of target hole investigations during the
192 Barnes maze probe trial across monomer- and PFF-injected mice of both sexes (Pearson's r = -
193 0.723, p = 0.0016; n = 16) (**Supplementary Fig. 4d**).

194 We next used the novel location recognition (NLR) test to assess spatial memory. The
195 novelty preference indices (NPIs) were calculated separately based on the time spent exploring or
196 the number of approaches toward the novel and familiar object locations. At 3MPI, during the first
197 minute of testing, the PFF-injected group exhibited a significantly lower time-based NPI than the
198 monomer-injected control group ($P = 0.0352$) (**Fig. 4f**). When calculated across the entire 5-min
199 test, the time-based NPI remained significantly lower in the PFF-injected group than in the
200 monomer-injected group ($P = 0.025$) (**Supplementary Fig. 3j**). The approach-based NPI showed
201 a similar pattern, although the overall treatment-group difference did not reach statistical
202 significance ($P = 0.0618$). Sex-stratified analysis revealed a significant difference between PFF-
203 and monomer-injected females ($P = 0.0165$) (**Fig. 4h**). No significant treatment-group differences
204 in either NPI measure were detected at 1MPI (**Fig. 4e, g**).

205 Novel object recognition (NOR) was then used to assess novelty recognition memory. At
206 1MPI, the PFF-injected group exhibited a significantly lower time-based object recognition NPI,
207 than the monomer-injected control group ($P = 0.0352$) (**Fig. 4i**). The approach-based novel object
208 NPI showed a similar pattern, although the overall treatment-group difference did not reach
209 statistical significance ($P = 0.0841$). Sex-stratified analysis revealed a significant treatment-group
210 difference in males ($P = 0.0074$) (**Fig. 4k**). At 3MPI, both NPI measures showed patterns similar
211 to those observed at 1MPI, but the differences between the PFF- and the monomer-injected groups
212 were not statistically significant (time-based NPI, $P = 0.0827$; approach-based NPI, $P = 0.1088$)
213 (**Fig. 4j, l**). Together, these findings demonstrate that PFF-induced α-syn pathology is associated

with selective cognitive deficits, including impaired target location memory in the Barnes maze at 1MPI, impaired novel location discrimination at 3MPI, and impaired novel object discrimination at 1MPI.

The α-synuclein PFF-injected mice exhibit increased risk assessment and anxiety-like behaviors

In addition to cognitive impairment, neuropsychiatric symptoms, including anxiety and disinhibition, are commonly observed in LBD patients [14]. We used the elevated zero maze (EZM) and open field test (OFT) to assess anxiety-like and risk-assessment behaviors at 1 and 3MPI. At 1MPI, PFF-injected mice showed a nonsignificant increase in the time spent in the open arms compared with monomer-injected controls ($P = 0.1335$), and the trend was stronger in females ($P = 0.052$) (**Fig. 5a**). By comparison, at 3MPI, PFF-injected mice spent significantly less time in the open arms than monomer-injected controls ($P = 0.0275$) (**Fig. 5b**). At 1MPI, PFF-injected females also exhibited a significant increase in the number of head dips ($P = 0.0006$), indicating reduced anxiety (**Fig. 5c**). In contrast, at 3MPI, both male and female PFF-injected mice exhibited significantly fewer head dips than their respective monomer-injected controls (**Fig. 5d**). Together, the open-arm time and head dip measurements suggest increased risk assessment or reduced anxiety-like behavior at 1MPI, followed by increased anxiety-like behavior at 3MPI.

Latency to first closed-arm entry, defined as the time required to enter a closed arm for the first time, was assessed, with a longer latency generally interpreted as reduced anxiety-like behavior. In accord with the open arm time and the head dip results, PFF- injected mice exhibited significantly longer closed-arm entry latency at 1MPI than monomer-injected controls ($P = 0.0494$). No significant treatment-group difference in latency to closed-arm entry was detected at

3MPI (**Fig. 5e, f**). The number of open arm entries did not differ significantly between the PFF- and the monomer-injected groups at either time point (**Fig. 5g, h**).

We further assessed anxiety-like behavior using the open field test (OFT) by measuring the time spent in the center, periphery, and corners, as well as the total distance traveled (**Fig. 5i-p**). Because behavior during the first 5 min can reflect the response to a novel environment and initial exploratory activity, we focused primarily on this interval. At 1MPI, PFF-injected females spent significantly less time in the corners than monomer-injected females ($P = 0.0482$), which may indicate reduced anxiety-like behavior/increased fearlessness. When both sexes were analyzed together, PFF-injected mice showed a trend towards a significant reduction in corner time ($P = 0.0567$) (**Fig. 5m**). No significant treatment-group differences were detected in the time spent in the center or periphery at either time point (**Fig 5i, j**). Furthermore, neither the distance traveled during the first 5 min or the full 30 min of the OFT nor grip strength differed significantly between the PFF- and monomer-injected groups, indicating that the observed behavioral differences were unlikely to be explained by alterations in locomotor activity or muscle strength (**Fig. 5o, p; Supplementary Fig. 2d and Supplementary Fig. 4b, c**). Together, these findings indicate that PFF-induced α-syn pathology is associated with time-dependent alterations in risk assessment and anxiety-like behavior. The behavioral profile at 1MPI was suggestive of reduced anxiety-like behavior or increased fearlessness, whereas the EZM results at 3MPI consistently indicated a transition into PFF-induced increased anxiety-like behavior.

Peripheral immune cell profiles differ by sex and time, with limited effects of PFF-induced α-syn pathology

To investigate whether PFF-induced α-syn pathology alters peripheral immune cell profiles, we performed flow cytometric analyses of the spleen, lymph nodes, and blood from bilaterally injected *Cx3cr1*^{GFP}/*Ccr2*^{RFP} mice and evaluated treatment-, sex-, and time-associated differences (**Fig. 6**). The gating strategy used to identify and quantify leukocyte populations is shown in Supplementary Figure 5. PFF-specific treatment effects were limited to the neutrophil population. Compared with monomer-injected controls, PFF-injected males exhibited a significantly lower neutrophil frequency in the spleen at 1MPI ($P = 0.0474$) (**Fig. 6a**) and in the lymph nodes at 3MPI ($P = 0.0234$) (**Fig. 6d**).

We next compared peripheral immune cell profiles between 1 and 3MPI within each treatment and sex (**Fig. 7**). In the spleen, the CD19$^+$ B cell population was significantly lower at 3MPI than at 1MPI in males from both treatment groups (Mono: $P = 0.0092$; PFF: $P = 0.0002$) (**Fig. 7a, b**). The splenic monocyte/macrophage population was also significantly reduced at 3MPI in PFF-injected males ($P = 0.0036$), whereas no significant difference was detected in PFF-injected females ($P = 0.1103$) (**Fig. 7a, b**).

In the lymph nodes, the NK cell population was significantly higher at 3MPI than at 1MPI in females from both treatment groups (Mono: $P = 0.0125$; PFF: $P = 0.0074$) (**Fig. 7c, d**). In the blood of monomer-injected females, CD3$^+$ T cell ($P = 0.014$) and CD4$^+$ T cell ($P = 0.0006$) populations were significantly lower at 3MPI. Similarly, PFF-injected females exhibited lower circulating CD3$^+$ ($P = 0.0022$), CD4$^+$ ($P = 0.0001$), and CD8$^+$ T cell ($P = 0.0135$) populations at 3MPI (**Fig. 7e, f**). In monomer-injected mice, the NK cell population was significantly higher at 3MPI in females but significantly lower at 3MPI in males. No significant temporal differences in NK cells were detected in PFF-injected mice (**Fig. 7e, f**). Together, these findings demonstrate that peripheral immune cell profiles differed primarily according to sex and time, whereas the specific

effect of PFF-induced α-syn pathology was restricted to reduced neutrophil frequencies in male mice.

Discussion

Intracranial injection of α-syn PFFs is commonly used to induce α-syn pathology in rodent models [18, 21, 29], producing pathology in regions, including the striatum, substantia nigra (SN), cortex, hippocampus, and brainstem depending on injection site [18, 27, 30]. The anatomical distribution of centrally injected PFF-induced pathology depends strongly on the injection site and its neuronal connections. For example, intrastriatal PFF injection induces α-syn aggregation within anatomically connected regions of the nigrostriatal system, including the SN, and has therefore widely used to model PD [19, 27], whereas intrahippocampal injection has been used to investigate α-syn pathology relevant to dementia with DLB. However, the extent to which PFF-induced α-syn pathology is accompanied by neuroinflammation, neuronal degeneration, and cognitive dysfunction varies across experimental models, and the consequences of intrahippocampal PFF injection remain comparatively understudied. In particular, few studies have examined whether hippocampal α-syn pathology is associated with CCR2+ monocyte infiltration or with alterations in peripheral immune cell populations. Furthermore, although biological sex may influence the clinical presentation and neuropathological features of LBDs, sex-related differences remain insufficiently characterized in experimental synucleinopathy models. To address these gaps, we characterized its neuropathological, immunological, and behavioral features at 1 and 3MPI. In our model, PFF-injected mice developed robust PK-resistant pSer129^{+} α-syn pathology in multiple hippocampal subfields, including DG, CA1, and CA3, as well as in the LEnt. We observed particularly pronounced α-syn pathology in the DG, a subfield that contributes to spatial memory,

pattern separation, and has also been implicated in anxiety-related behavior [31, 32]. A Postmortem study of DLB identified α-syn pathology in the hippocampus and entorhinal cortex, with greater CA1 pathology associated with poorer memory performance [7]. Hippocampal and lenticular involvement in our model therefore overlaps with regions affected in human DLB, although the relative subfield distribution may differ. Consistent with a link between regional pathology and memory, DG pSer129^{+} area was negatively correlated with Barnes maze target hole investigations. Together, these findings support the relevance of the affected regions to LBD-related memory dysfunction.

Exogenously administered α-syn PFFs can recruit endogenous α-syn and facilitate aggregation [15, 16], and in vitro studies indicate that endogenous α-syn expression influences the extent of PFF-induced aggregation [15, 17]. To examine this requirement in vivo, we injected α-syn PFF into the hippocampus of WT and α-syn-knockout (Syn KO) mice. Robust PK-resistant pSer129^{+} α-syn pathology was detected in WT mice, but was absent in Syn KO mice at 5 MPI, indicating that the observed pathology reflects recruitment and aggregation of endogenous α-syn rather than residual injected fibrils.

Neuroinflammation is an important feature of synucleinopathies, and several studies have reported increased microglial and astrocytic responses in association with α-syn pathology [18, 20, 22, 27]. Nevertheless, glial responses to PFF-induced α-syn pathology have been less extensively characterized in the hippocampus and other LBD-relevant regions than in the nigrostriatal system. In our unilaterally injected model, PFF-induced α-syn pathology increased both Iba-1^{+} and GFAP^{+} areas in the DG, and increased Iba-1^{+} area in the CA3. These results indicate regionally distinct glial responses, with the DG exhibiting both microglial and astrocytic changes and CA3 exhibiting a predominantly microglial change under the conditions examined. A previous study reported

astroglial reactivity in the CA2/3 subfield following forebrain α-syn PFF injection [21], however, comparatively little is known about concurrent microglial and astrocytic responses in the DG. Bilaterally injected *Cx3cr1*^{GFP}/*Ccr2*^{RFP} mice exhibited increased CX3CR1^{+} area in the DG, CA1, and CA3; because these cohorts differ in injection laterality, mouse line, and detection method, the two datasets are not directly comparable. Glial activation is also a feature of human LBD. Postmortem studies have described reactive microglia and astrocytes in association with Lewy pathology in DLB, and in vivo imaging has detected microglial activation in patients with DLB [33-35]. The concurrent microglial and astrocytic responses observed here therefore parallel glial responses reported in human disease, although the regional distribution in our model may not fully correspond to that described in patients. Given the prominent α-syn pathology and neuronal degeneration observed in the DG, the accompanying increases in Iba-1, CX3CR1, and GFAP immunoreactivity suggest that this hippocampal subfield is particularly affected in our model.

CCR2^{+} monocytes have been implicated in neuroinflammation in experimental synucleinopathy models [23, 24]. Genetic deletion of CCR2 prevented peripheral monocyte recruitment to the CNS and attenuated neuroinflammation and neurodegeneration in an α-syn overexpression model of PD [23], indicating that recruited monocytes can contribute to disease processes rather than simply accompanying them. In the present study, PFF-injected mice showed increased CCR2^{+} area in the DG and CA1, consistent with CCR2^{+} monocyte recruitment to regions bearing α-syn pathology. Notably, some CCR2^{+} cells in the DG also expressed CX3CR1. In the reporter study by Saederup et al., resident microglia expressed CX3CR1 but lacked detectable CCR2 reporter expression, including during EAE [25], supporting the interpretation that the double-positive cells observed in our study represent a recruited myeloid population rather than resident microglia. A comparable phenotypic transition has been described following an acute

ischemic stroke in which recruited pro-inflammatory CCR2^{high}CX3CR1^{low} monocytes gradually acquired an anti-inflammatory CCR2^{low}CX3CR1^{high} macrophage phenotype associated with inflammation resolution and tissue repair [28, 36]. However, that transition was characterized in an acute injury setting, and reporter coexpression alone does not establish that a similar adaptation, or a similarly reparative function, occurs in chronic α-syn-associated pathology.

The relative contributions of recruited monocytes and resident glia to hippocampal PFF-induced pathology remain unclear. In an α-syn PFF model, inhibition of microglia-mediated induction of neurotoxic astrocyte responses reduced neuronal loss and behavioral deficits, supporting a pathogenic contribution of interactions between these resident glial populations [26]. Our findings suggest that CCR2^{+} cell accumulation occurs alongside resident glial responses, but do not establish whether these cells amplify inflammation, support repair, or change function over time. Further phenotypic characterization, together with experiments targeting monocyte recruitment or specific microglial and astrocytic responses, will be needed to determine how each of these populations contribute to neuronal injury and repair.

Cognitive impairment is a prominent nonmotor symptom of LBD [2], and deficits in spatial recognition memory have been documented in patients with autopsy-confirmed DLB [37]. Hippocampal α-syn pathology has also been associated with memory impairment in human DLB [7]. In the present study, hippocampal α-syn PFF-induced pathology was associated with selective cognitive deficits that varied across tasks and time points. Although PFF-injected mice showed no impairment in Barnes maze acquisition, they investigated the target hole less frequently during the probe trial at 1 MPI, suggesting impaired memory for the previously learned target location [38]. The negative correlation between DG pSer129^{+} α-syn area and target hole investigations at 1 MPI further supports an association between DG pathology and spatial memory performance. However,

because this analysis included both treatment groups, the relationship may partly reflect between-group differences and does not establish causality. The longer distance traveled to find the target hole at 3MPI may indicate less efficient searching, although it remains unclear whether spatial learning was impaired.

The NOR and NLR findings suggest that recognition memory was also affected, with deficits detected at different time points. PFF-injected females showed a significant impairment in novel-location discrimination at 3MPI, as indicated by both time- and approach-based novelty preference indices. Clinical studies have also identified sex-associated differences in cognition. For example, females with Lewy body pathology showed a faster increase in the prevalence of visuospatial deficits and dementia severity during the prodromal period than males [11]. More broadly, our results are consistent with clinical evidence linking hippocampal α-syn pathology to memory impairment [7] and experimental studies showing that hippocampal synucleinopathy disrupts memory-related functions [21, 39]. Forebrain PFF injection has been shown to produce progressive spatial learning and memory deficits accompanied by hippocampal α-syn pathology and neurodegeneration [21]. Similarly, selective overexpression of human α-syn in the dorsal hippocampus resulted in early and persistent memory impairment associated with disrupted hippocampal synaptic plasticity [39].

The different findings across behavioral tasks may reflect the types of memory each task assesses. The Barnes maze assesses spatial learning and memory through target-directed searching using environmental cues [38], whereas NLR tests recognition of a changed object location [40]. NOR primarily assesses discrimination between novel and familiar objects and depends strongly on the perirhinal cortex, while hippocampal involvement is more evident when recognition memory requires spatial or temporal information [40, 41]. Thus, deficits in some behavioral

measures but not others do not necessarily indicate an inconsistent phenotype. Instead, it may suggest that PFF-induced α-syn pathology preferentially affects specific components of memory processing.

In addition to cognitive deficits, PFF-injected mice exhibited alterations in risk-assessment and anxiety-like behaviors that differed between time points. At 1 MPI, increased head dipping in PFF-injected females, together with a nonsignificant tendency toward greater open-arm exploration, longer closed-arm latency, and reduced corner occupancy, was generally consistent with decreased anxiety-like behavior/ increased fearlessness behavior. Head dipping provides an additional measure of exploration in an exposed environment [42], while the longer closed-arm entry latency suggested reduced initial retreat to a protected area. Several early behavioral differences were detected in females, although these findings alone do not establish different treatment responses between sexes. In a clinical study of prodromal DLB, disinhibition was more frequent in females two years before diagnosis, but the number of affected participants was small [12]. At 3 MPI, PFF-injected mice spent less time in the open arms and exhibited fewer head dips, providing more consistent evidence of increased anxiety-like behavior. Anxiety is also clinically relevant across synucleinopathies, with a meta-analysis reporting higher prevalence and greater severity in females, although the evidence was predominantly derived from PD studies [14]. Likewise, experimental α-syn models have produced heterogeneous anxiety-related phenotypes. For example, intrastriatal PFF injection has been associated with reduced anxiety-like behavior in the light-dark box [43], and α-syn overexpressing transgenic mice have exhibited greater open-arm exploration and reduced anxiety-like behavior [44]. In contrast, long-term α-syn overexpression originating in the midbrain has been associated with increased avoidance behavior and broader emotional and cognitive dysfunction [39]. Together, these findings suggest that the

anxiety-related behavioral consequences of α-syn pathology depend on the affected neural circuits, the experimental model, and the time of assessment.

Although little to no α-syn pathology was detected in the amygdala, hippocampal dysfunction may contribute to the observed anxiety-related behaviors. Experimental studies have demonstrated roles for DG activity in exploration and anxiety regulation [32] and for ventral hippocampal circuits in anxiety-related avoidance [45]. These studies suggest that hippocampal dysfunction could contribute to the anxiety-related behaviors observed in our mice, although the specific mechanisms remain unclear. Furthermore, locomotor activity and grip strength did not differ significantly between treatment groups, suggesting that differences in movement or muscle strength were unlikely to explain the observed cognitive and anxiety-related behaviors.

Peripheral immune cell profiles showed limited treatment-specific alterations following hippocampal α-syn PFF injection. Our results show a lower neutrophil frequency in PFF-injected males, detected in the spleen at 1 MPI and the lymph nodes at 3 MPI. Previous work has demonstrated that intracranially initiated α-syn pathology can alter immune cell profiles in peripheral lymphoid organs, although the affected populations vary across models [18]. The tissue- and time-dependent neutrophil changes observed here may reflect altered neutrophil homeostasis or redistribution among peripheral compartments [46]. However, because we measured relative frequencies rather than absolute cell numbers, these findings do not establish systemic neutrophil depletion or altered neutrophil function. Most other immune changes were associated with time and occurred in both monomer- and PFF-injected mice. These included reduced splenic B cell frequencies in males, increased lymph node NK cell frequencies in females, and reduced circulating T cell frequencies in females at 3MPI. Previous studies have similarly demonstrated that peripheral immune cell composition changes with age and that the magnitude and direction of

these changes differ between males and females [47, 48]. Therefore, changes appeared both in the monomer and PFF groups may reflect normal age-related immune variation, time after surgery, or other experimental factors rather than PFF-induced α-syn pathology. Overall, these findings indicate that sex and time are important sources of variation in peripheral immune composition, whereas the treatment-specific effect of PFF-induced pathology was comparatively limited and primarily involved neutrophils in males.

Several limitations should be considered when interpreting these findings. While this study characterized hippocampal α-syn pathology, glial responses, neuronal degeneration, and behavioral alterations, it did not determine the causal relationships between these tissue changes and behavioral outcomes. The negative correlation between DG α-syn pathology and Barnes maze target hole investigations supports an association but does not establish causality. Similarly, the reporter system enabled visualization of $CCR2^{+}$ cells but did not establish whether these cells contribute to hippocampal pathology.

Our findings demonstrate that single hippocampal PFF injection produces persistent, endogenous α-syn-dependent pathology accompanied by regionally selective neuronal and glial changes, $CCR2^{+}$ cell accumulation, and selective cognitive and anxiety-related behavioral alterations. Peripheral immune profiles showed sex- and time-associated patterns, with comparatively limited PFF-specific effects. Together, these findings support the utility of this model for studying selected neuropathological and nonmotor features relevant to LBD and provide a basis for testing how hippocampal pathology and immune responses contribute to behavioral dysfunction.

Methods and Materials

Mice

C57BL/6J mice (wild-type; WT) were initially purchased from the Jackson Laboratory (#000664) and were bred in the central animal facility at the University of Georgia. *Cx3cr1*^{GFP}/*Ccr2*^{RFP} mice (Jackson Laboratory, Strain # 032127) or *Snca*-knockout (Syn KO) mice (Jackson Laboratory, Strain # 016123) were also used. Mice were housed in a climate-controlled facility with a 12-hour light-dark cycle (light cycle 7:00 - 19:00). All research was performed in accordance with the latest NIH Guidelines for Animal Care and Use and approved in advance by the Institutional Animal Care and Use Committee at the respective institution, the University of Georgia or Rutgers University.

Three independent cohorts were used for the unilateral hippocampal injection experiments. Cohort 1 comprised monomer-injected controls and PFF-injected mice assessed at 3MPI (n = 4 per group). Cohort 2 comprised PFF-injected mice assessed at 1MPI (n = 4). Cohort 3 comprised monomer-injected controls assessed at 3MPI and PFF-injected mice assessed at 1 or 3MPI (n = 4 per group). For the bilateral hippocampal injection experiments, male and female *Cx3cr1*^{GFP}/*Ccr2*^{RFP} mice received α-syn monomers or PFFs and were assessed at 1 or 3MPI. The 1MPI cohort comprised 8 monomer-injected mice (4 males and 4 females) and 9 PFF-injected mice (4 males and 5 females). The 3MPI cohort comprised 11 monomer-injected mice (5 males and 6 females) and 11 PFF-injected mice (6 males and 5 females). A separate cohort assessed at 5MPI comprised 8 WT (4 males and 4 females) and 7 Syn KO mice (3 males and 4 females).

Recombinant α-synuclein and fibril preparation

Recombinant human α-synuclein and fibrils were generated as previously described [49]. Recombinant human α-Syn was expressed in E. coli BL21(DE3)/RIL cells and purified to >98 %

purity via size exclusion chromatography, Mono Q ion exchange chromatography, and finally by High S cation exchange chromatography, as previously described [50, 51]. Endotoxin levels were confirmed to be below 0.5 EU/mg. To confirm adequate endotoxin removal, the QUANTI-BlueTM assay was performed using HEK-BlueTM TLR4 reporter cells to determine TLR4-mediated NF-kB activation. To generate pre-formed fibrils (PFFs), purified recombinant α-Syn monomers (5.49 mg/mL) were incubated at 37 °C with constant shaking (1100 rpm) for 7 days. Immediately prior to stereotaxic injection, fibrils were sonicated (Qsonica Q700, 30% amplitude) for 30 minutes using a cycle of 3 seconds on and 2 seconds off. PFF morphology and seed size were validated using transmission electron microscopy (TEM) as previously described [49].

Stereotaxic Injection

3-month-old male and female WT or *Cx3cr1*^{GFP}/*Ccr2*^{RFP} mice were anesthetized with isoflurane (5% induction, 1-2% maintenance) and fixed to a stereotaxic frame (David KOPF Instruments, Tujunga, CA, USA). Animals then received unilateral or bilateral sterile injections of human α-syn PFF (5μg) or monomeric α-syn (5μg) into the hippocampus: AP: -2.5, ML: ±2.0, DV: -1.8. A 29-gauge Hamilton syringe was used to perform these injections at a rate of 0.2 μL/min. Animals were monitored for pain and discomfort for 7 days and received analgesics subcutaneously for 3 days after the procedure.

Behavioral Assessment

1- or 3-months post-injection, mice underwent a battery of behavioral tests for the assessment of memory, motor, and mood function. Mice were acclimated to the testing room before the experiment began. All behavioral tests were carried out between 7:00 am and 11:30 am.

All tests and analyses were conducted in a treatment-blind manner in the sequence depicted in Supplemental Figure 4a.

Elevated Zero Maze (EZM)

The elevated zero maze was used to assess anxiety-like behavior [52] on day 1. After a 10-minute room habituation, mice were placed in the center of an open arm of the EZM apparatus (Stoelting Co., Wood Dale, IL), which was illuminated by a dim red light in a dark room. The mice then freely explored for 5 minutes. Recordings of the test were used to score time spent in the open arms (which required 70% of a mouse's body to be in the zone), latency to first enter a closed arm, and head dips in ANY-Maze (Stoelting) [53].

Open Field Test (OFT)

The open field test was used to assess motor and anxiety-like behaviors, as per [54], on day 3. After 10-minute room habituation, mice were placed in the center of a 25 cm x 25 cm open field (Coulbourn Instruments, Whitehall, PA) and allowed to explore freely for 30 minutes. Entries into and time spent in the periphery, center, and corners of the apparatus, as well as distance travelled, was scored automatically using ANY-Maze. The number of rearing events was scored using Limelight 3 (Actimetrics, Wilmette, IL).

Novel Location Recognition

We performed the novel location recognition test to assess spatial memory on day 4. The previous day's OFT served as habituation to the apparatus. After a 10-minute habituation to the testing room, mice were placed in the open field with two identical objects in the corners on the

same side and were allowed to explore freely for 5 minutes. Mice were then returned to their home cage for 1 hour, then placed back into the apparatus with one object in its initial position, and the other object moved to a novel location in the adjacent corner. Mice were then allowed to explore freely for 5 minutes. The number of approaches and time spent investigating the familiar and novel locations was scored using Limelight 3 (Actimetrics) [53]. For both NLR and NOR, the novelty preference index (NPI) was calculated as exploration of the novel object or location divided by total exploration of the novel and familiar objects or locations, multiplied by 100. NPIs were calculated separately using exploration time and the number of approaches. An NPI of 50% indicates equal preference, whereas values above or below 50% indicate greater preference for the novel or familiar object or location, respectively.

Novel Object Recognition

24 hours following the novel location recognition test, mice were placed back into the apparatus, but with the identical object that was previously in the novel location replaced with a novel object. Mice were again allowed to freely explore for 5 minutes. The number of approaches and time spent investigating the familiar and novel object was scored using Limelight 3 (Actimetrics) [53].

Barnes Maze

The Barnes maze (Stoelting), a brightly lit, elevated circular apparatus with 20 holes around its edge, was used to assess spatial learning and memory [55]. One of these 20 holes led to an escape box, where mice could escape the apparatus's anxiogenic nature. The hole that led to the escape box is referred to as the target hole (TH). On day 7, mice were habituated to the apparatus

by placing them in the center and gently guiding them to the TH. The acquisition phase took place on days 8-11, where mice learned to find the TH over 4 3-minute trials per day. If a mouse did not enter the TH after 3 minutes, it was gently guided to the TH. After each trial, mice remained in the TH for 1 minute. Between mice, we rotated and sanitized the apparatus to remove olfactory cues. The probe trial took place on day 12, where the escape box was removed, and the mice were allowed to explore the apparatus once for 90 seconds. We used an ANY-Maze (Stoelting) to track and score the number of errors, distance to the TH, time to find the TH, and search strategy for each acquisition trial. Number of TH investigations, distance travelled until first TH investigation, and time until first TH investigation was tracked and scored for the probe trial [53].

Grip Strength

After a 2-hour rest following the probe trial, forelimb grip strength was measured over 4 trials to assess motor performance using a gauge with a purpose-built wire grid (Bioseb, France). The inter-trial interval was 3 minutes. Average and maximal grip strength were assessed.

Sample preparation

Mice were euthanized and transcardially perfused with 0.1 M phosphate-buffered saline (PBS). Brains were collected, bisected midsagittally, and the right half was immersion-fixed in 4 % paraformaldehyde for 48 hours. Next, brains were dehydrated in 30 % sucrose until sunk, flash-frozen in isopentane (2-methylbutane) on dry ice, and stored at -80 °C until sectioned with a cryostat. The brains were sectioned coronally at 30 µm and stored in 0.1 M PBS with 0.05 % sodium azide.

Immunohistochemistry

The sections were treated with proteinase K (10 ug/mL; MP Biomedicals, 183988) for 5 min, followed by incubation in 3 % H_2O_2 (Fisher Chemical) to quench the endogenous peroxidase activity. Sections were then blocked in 0.1 M Tris-Buffered saline (TBS) containing avidin (10 µg/mL, Vector Laboratories), 8 % normal goat serum (Sigma), 0.1 % TritonX-100 (Bio-Rad). Sections were incubated overnight at 4 °C with an antibody against a-syn phosphorylated at serine 129 (pSer129) (Abcam, ab51253, 1:25,000) diluted in 0.1 M TBS containing biotin (50 µg/mL; Vector Labs), 2 % normal serum (Sigma). Subsequently, sections were incubated with biotinylated secondary antibody (Vector Labs) diluted in 0.1 M TBS containing 2 % normal serum for 1 hour at 4 °C. Signal was developed using a standard VectaStain Elite ABC peroxidase kit (Vector Laboratories) for 1 hour at 4 °C, followed by incubation with 3, 3'-diaminobenzidine (DAB) (Vector Laboratories) for 2 min. Sections were mounted on gelatin-subbed slides (SouthernBiotech), dehydrated through 70 %, 95 %, and 100 % ethanol, and cleared in histoclear (HS-200). Slides were coverslipped using VectaMount Express mounting medium (Vector Laboratories, H-5700-60).

Immunofluorescence

Brain sections underwent antigen retrieval by incubation in citrate buffer (0.1 M citric acid and 0.1 M tris-sodium citrate) at 60°C overnight. Antigen retrieval was omitted for sections from *Cx3cr1*^{GFP}/*Ccr2*^{RFP} mice. Sections were washed three times with 0.1 M phosphate-buffered saline (PBS) and incubated in 0.2 M glycine in PBS for 1 hour. Sections were then permeabilized in 0.1 M TBS containing 1 % normal serum and 0.3 % TritonX-100 for 35 min at room temperature. Following three PBS washes, sections were blocked with 1 % normal serum for 1 hour at room

604 temperature. Sections were incubated overnight at 4 °C with the appropriate primary antibodies or
605 reagent diluted in 0.1 M TBS containing 1 % normal serum and 0.1 % TritonX-100. Primary
606 antibodies included anti-NeuN (Synaptic Systems, 266 004; 1:400), anti-GFAP (Synaptic Systems,
607 173 004; 1:1000), anti-Iba-1 (Wako, 019-19741; 1:500), and anti-pSer129 (Wako, 015-25191, or
608 Abcam, ab51253; 1:25,000). Fluoro-Jade C (Biosensis, TR-160-FJC; 0.00005%) was used for
609 neuronal degeneration staining under the same incubation conditions. The following day, sections
610 were washed with TBST (0.05 % TritonX-100 in 0.1 M TBS) and incubated for 2 hours at room
611 temperature with Alexa Flour®488-, 555-, or 647-conjugated secondary antibodies (Jackson
612 Laboratory; 1:1000) diluted in 0.1 M TBS containing 1 % normal serum and 0.1 % Triton X-100.
613 Sections were subsequently washed with TBST and distilled water, counterstained with Hoechst
614 (Invitrogen, H3569; 1:10,000) for 5 min, and washed with distilled water. Sections were stored in
615 0.1 M PBS until mounting and coverslipping with antifade mounting medium (Invitrogen, P36930).
616
617 **Imaging and Quantitative Analysis**
618 Images of the hippocampus, lateral entorhinal cortex (LEnt), amygdala, and prefrontal
619 cortex were acquired at 20X magnification using a Keyence BZ-X800 microscope (Keyence,
620 Osaka, Japan). Brain sections from one hemisphere of each *Cx3cr1*^{GFP}/*Ccr2*^{RFP} mouse were used
621 for staining, imaging, and quantification. Images were stitched to generate composite images of
622 each section. Quantitative analysis was performed using ImageJ software (version 1.54; National
623 Institute of Health). Images were converted to 8-bit grayscale and thresholded to exclude
624 background signal. Regions of interest (ROIs) were manually delineated within each brain region,
625 and the immunoreactive area within each ROI was measured. For each brain region, the mean
626 immunoreactive area across sections was calculated for each animal.

627

628 **Flow Cytometry**

629 Spleen cells were isolated from mice, treated with ACK lysing buffer (Quality Biological,
630 Cat# 118-156-101) to remove red blood cells, and then washed in 1X PBS. Cells were then
631 incubated for 20 minutes at 4°C with TruStain FcX™ anti-mouse CD16/32 antibody (BioLegend,
632 Cat# 101319, 1:100) to block Fc receptors. Subsequently, cells were stained and incubated with
633 several fluorophore conjugated antibodies including CD45 Pacific Blue (Cat# 103126, 1;400),
634 CD3 BV711 (Cat# 100241, 1:200), CD4 PE Cy5 (Cat# 100410, 1:200), CD8 APC Cy7 (Cat#
635 100714, 1:200), CD19 APC (Cat# 115512, 1:200), Ly6C BV570 (Cat# 128030, 1:200), NK1.1 PE
636 Cy7 (Cat# 156514, 1:200), CD14 BV605 (Cat# 123335, 1:200), CD11b BV785 (Cat# 101208,
637 1:200) and Ly6G AF700 (Cat# 56-593182, 1:200). All antibodies were purchased from Biolegend
638 (San Diego, CA) except for Ly6G which was purchased from eBioscience, ThermoFisher
639 Scientific (Carlsbad, CA). Cells were sorted and data were acquired using a Novo Agilent
640 Quanteon (4 laser, 24 colors) (Santa Clara, CA). Data were analyzed with Novoexpress software
641 version 1.5.6. The frequency of various immune cellular entities in the spleen and lymph nodes
642 was then calculated by taking into account the percentage of the immune entity within the total
643 lymphocytes. Frequencies of immune cells based on treatment were compared using GraphPad
644 Prism 11 (San Diego, CA).

645

646 **Statistical Analysis**

647 Statistical analyses were performed using GraphPad Prism 11 (San Diego, CA). Data are
648 presented as the mean ± SEM. Comparisons among treatment groups and time points were
649 conducted using ordinary one-way ANOVA followed by Tukey's multiple comparisons test, or

Brown-Forsythe and Welch ANOVA followed by Dunnett's T3 multiple comparisons test, as appropriate. Comparisons between two independent treatment groups were performed using a two-tailed unpaired Student's t-test or the Mann-Whitney *U* test, as appropriate. Two-way ANOVA followed by Fisher's least significant difference (LSD) test was used to evaluate the effects of treatment and sex or time point and sex, including their interactions. Barnes maze acquisition data were analyzed separately on each acquisition day using two-way ANOVA with sex and treatment as factors, including the sex x treatment interaction. For these acquisition analyses, Student-Neumann-Keuls post hoc comparisons were used to assess sex differences when appropriate. Pearson's correlation coefficients (r) were calculated to assess linear associations between the number of target hole investigations in the Barnes maze and total pSer129^{+} area. Statistical significance was defined as $P < 0.05$. Individual P values are reported in the Results, and figure legends define the significance thresholds represented by asterisks.

Acknowledgements
This study was supported by awards to J.K.L. by the NIH R01NS119610. We also thank Dr. Jason Richardson and Dr. Hyojung Choo for providing access to the Keyence microscope for imaging.

Author Contributions
J.K.L. and N.F. conceived and supervised this study. J.H.B. performed the in vivo experiments, analyzed all immunohistochemistry and immunofluorescence data, and drafted the manuscript. B.H. performed in vivo experiments, analyzed all behavioral data, and drafted the manuscript. D.G. conducted stereotaxic surgeries. A.A. performed flow cytometry and analyzed data. J.L. performed immunohistochemistry and immunofluorescent staining. J.C. contributed to experimental supervision and performed flow cytometry. W.H.C. and Y.S.K. performed in vivo experiments for 5MPI data in KO mice. J.K.L., N.F., J.H.B., and B.H. wrote the manuscript, with contributions from all authors.
J.H.B. and B.H. equally contributed to this work.
Corresponding to J.K.L. and N.F.

Competing interests
J.K.L. serves as a scientific advisor for Neuronity Therapeutics, Inc. All other authors declare no competing interests.

Additional information
Supplementary information. The online version contains supplementary material available at:

Data Availability
Data supporting the findings of this study are presented in this article and its supplementary information files. The underlying datasets are available from the corresponding authors upon request.

References

1. Neef, D. and A.D. Walling, *Dementia with Lewy bodies: an emerging disease.* Am Fam Physician, 2006. **73**(7): p. 1223-9.
2. McKeith, I.G., et al., *Diagnosis and management of dementia with Lewy bodies: Fourth consensus report of the DLB Consortium.* Neurology, 2017. **89**(1): p. 88-100.
3. Vann Jones, S.A. and J.T. O'Brien, *The prevalence and incidence of dementia with Lewy bodies: a systematic review of population and clinical studies.* Psychol Med, 2014. **44**(4): p. 673-83.
4. Kane, J.P.M., et al., *Clinical prevalence of Lewy body dementia.* Alzheimer's Research & Therapy, 2018. **10**(1): p. 19.
5. Mouton, A., et al., *Sex ratio in dementia with Lewy bodies balanced between Alzheimer's disease and Parkinson's disease dementia: a cross-sectional study.* Alzheimer's Research & Therapy, 2018. **10**(1): p. 92.
6. Rau, A., et al., *Hippocampus and basal forebrain degeneration differentially impact cognition in Lewy body spectrum disorders.* Brain, 2025. **148**(8): p. 2772-2784.
7. Adamowicz, D.H., et al., *Hippocampal α-Synuclein in Dementia with Lewy Bodies Contributes to Memory Impairment and Is Consistent with Spread of Pathology.* The Journal of Neuroscience, 2017. **37**(7): p. 1675-1684.

8. Chiu, S.Y., et al., *Sex differences in dementia with Lewy bodies: Focused review of available evidence and future directions.* Parkinsonism Relat Disord, 2023. **107**: p. 105285.
9. Bayram, E., et al., *Sex Differences for Social Determinants Associated with Lewy Body Dementia Onset and Diagnosis.* Neurodegenerative Diseases, 2025. **25**(1): p. 1-13.
10. Lange, R., et al., *Do sex differences in dementia with Lewy bodies arise from Alzheimer's disease biological profile?* J Alzheimers Dis, 2026. **109**(4): p. 1621-1624.
11. Tsai, A., et al., *Sex differences for symptoms prior to dementia onset in people with Lewy body pathology compared to pure Alzheimer's disease pathology.* J Alzheimers Dis, 2026. **109**(3): p. 1188-1199.
12. Wyman-Chick, K.A., et al., *Sex differences in prodromal dementia with Lewy bodies using the National Alzheimer's Coordinating Center data.* Alzheimers Dement, 2025. **21**(5): p. e70275.
13. Bayram, E., et al., *Sex differences for regional pathology in people with a high likelihood of Lewy body dementia phenotype based on underlying pathology.* Alzheimers Dement (Amst), 2025. **17**(1): p. e70083.
14. Couture, V., et al., *Sex Differences in Neuropsychiatric Symptoms in Alpha-Synucleinopathies: A Systematic Review and Meta-Analysis.* Movement Disorders Clinical Practice, 2024. **11**(11): p. 1335-1344.
15. Volpicelli-Daley, L.A., K.C. Luk, and V.M. Lee, *Addition of exogenous α-synuclein preformed fibrils to primary neuronal cultures to seed recruitment of endogenous α-synuclein to Lewy body and Lewy neurite-like aggregates.* Nat Protoc, 2014. **9**(9): p. 2135-46.
16. Wu, Q., et al., *α-Synuclein (αSyn) Preformed Fibrils Induce Endogenous αSyn Aggregation, Compromise Synaptic Activity and Enhance Synapse Loss in Cultured Excitatory Hippocampal Neurons.* The Journal of Neuroscience, 2019. **39**(26): p. 5080.
17. Vasili, E., et al., *Endogenous Levels of Alpha-Synuclein Modulate Seeding and Aggregation in Cultured Cells.* Mol Neurobiol, 2022. **59**(2): p. 1273-1284.
18. Earls, R.H., et al., *Intrastriatal injection of preformed alpha-synuclein fibrils alters central and peripheral immune cell profiles in non-transgenic mice.* J Neuroinflammation, 2019. **16**(1): p. 250.
19. Stoll, A.C. and C.E. Sortwell, *Leveraging the preformed fibril model to distinguish between alpha-synuclein inclusion- and nigrostriatal degeneration-associated immunogenicity.* Neurobiol Dis, 2022. **171**: p. 105804.
20. Sacino, A.N., et al., *Brain injection of α-synuclein induces multiple proteinopathies, gliosis, and a neuronal injury marker.* J Neurosci, 2014. **34**(37): p. 12368-78.
21. Dues, D.J., et al., *Hippocampal subfield vulnerability to α-synuclein pathology precedes neurodegeneration and cognitive dysfunction.* NPJ Parkinsons Dis, 2023. **9**(1): p. 125.
22. Garcia, P., et al., *Neurodegeneration and neuroinflammation are linked, but independent of alpha-synuclein inclusions, in a seeding/spreading mouse model of Parkinson's disease.* Glia, 2022. **70**(5): p. 935-960.
23. Harms, A.S., et al., *Peripheral monocyte entry is required for alpha-Synuclein induced inflammation and Neurodegeneration in a model of Parkinson disease.* Exp Neurol, 2018. **300**: p. 179-187.
24. Xu, E., et al., *Pathological α-synuclein recruits LRRK2 expressing pro-inflammatory monocytes to the brain.* Mol Neurodegener, 2022. **17**(1): p. 7.

25. Saederup, N., et al., *Selective chemokine receptor usage by central nervous system myeloid cells in CCR2-red fluorescent protein knock-in mice.* PLoS One, 2010. **5**(10): p. e13693.
26. Yun, S.P., et al., *Block of A1 astrocyte conversion by microglia is neuroprotective in models of Parkinson's disease.* Nature Medicine, 2018. **24**(7): p. 931-938.
27. Adebowale, A., et al., *Adoptive NK cell transfer confers neuroprotection by attenuating neuroinflammation and alpha-synuclein pathology in a mouse model of synucleinopathy.* Molecular Neurodegeneration Advances, 2025. **1**(1): p. 6.
28. Park, J., et al., *Reparative System Arising from CCR2(+) Monocyte Conversion Attenuates Neuroinflammation Following Ischemic Stroke.* Translational Stroke Research, 2021. **12**(5): p. 879-893.
29. Luk, K.C., et al., *Pathological α-Synuclein Transmission Initiates Parkinson-like Neurodegeneration in Nontransgenic Mice.* Science, 2012. **338**(6109): p. 949-953.
30. Verma, D.K., et al., *Alpha-Synuclein Preformed Fibrils Induce Cellular Senescence in Parkinson's Disease Models.* Cells, 2021. **10**(7): p. 1694.
31. McHugh, T.J., et al., *Dentate Gyrus NMDA Receptors Mediate Rapid Pattern Separation in the Hippocampal Network.* Science, 2007. **317**(5834): p. 94-99.
32. Kheirbek, Mazen A., et al., *Differential Control of Learning and Anxiety along the Dorsoventral Axis of the Dentate Gyrus.* Neuron, 2013. **77**(5): p. 955-968.
33. McGeer, P.L., et al., *Reactive microglia are positive for HLA‐DR in the substantia nigra of Parkinson's and Alzheimer's disease brains.* Neurology, 1988. **38**(8): p. 1285-1285.
34. Surendranathan, A., et al., *Early microglial activation and peripheral inflammation in dementia with Lewy bodies.* Brain, 2018. **141**(12): p. 3415-3427.
35. Iannaccone, S., et al., *In vivo microglia activation in very early dementia with Lewy bodies, comparison with Parkinson's disease.* Parkinsonism & Related Disorders, 2013. **19**(1): p. 47-52.
36. Gliem, M., M. Schwaninger, and S. Jander, *Protective features of peripheral monocytes/macrophages in stroke.* Biochimica et Biophysica Acta (BBA) - Molecular Basis of Disease, 2016. **1862**(3): p. 329-338.
37. Salmon, D.P., et al., *Recognition memory span in autopsy-confirmed Dementia with Lewy Bodies and Alzheimer's Disease.* Neuropsychologia, 2015. **75**: p. 548-555.
38. Illouz, T., et al., *Unbiased classification of spatial strategies in the Barnes maze.* Bioinformatics, 2016. **32**(21): p. 3314-3320.
39. Iemolo, A., et al., *Synaptic mechanisms underlying onset and progression of memory deficits caused by hippocampal and midbrain synucleinopathy.* npj Parkinson's Disease, 2023. **9**(1): p. 92.
40. Barker, G.R.I. and E.C. Warburton, *When Is the Hippocampus Involved in Recognition Memory?* The Journal of Neuroscience, 2011. **31**(29): p. 10721.
41. Barker, G.R.I., et al., *Recognition Memory for Objects, Place, and Temporal Order: A Disconnection Analysis of the Role of the Medial Prefrontal Cortex and Perirhinal Cortex.* The Journal of Neuroscience, 2007. **27**(11): p. 2948.
42. Shepherd, J.K., et al., *Behavioural and pharmacological characterisation of the elevated "zero-maze" as an animal model of anxiety.* Psychopharmacology, 1994. **116**(1): p. 56-64.
43. Alwani, A., et al., *Investigating the potential effects of α-synuclein aggregation on susceptibility to chronic stress in a mouse Parkinson's disease model.* Pharmacological Reports, 2023. **75**(6): p. 1474-1487.

44. George, S., et al., *α-Synuclein transgenic mice exhibit reduced anxiety-like behaviour.* Experimental Neurology, 2008. **210**(2): p. 788-792.
45. Jimenez, J.C., et al., *Anxiety Cells in a Hippocampal-Hypothalamic Circuit.* Neuron, 2018. **97**(3): p. 670-683.e6.
46. Casanova-Acebes, M., et al., *Rhythmic Modulation of the Hematopoietic Niche through Neutrophil Clearance.* Cell, 2013. **153**(5): p. 1025-1035.
47. Menees, K.B., et al., *Sex- and age-dependent alterations of splenic immune cell profile and NK cell phenotypes and function in C57BL/6J mice.* Immunity & Ageing, 2021. **18**(1): p. 3.
48. Serre-Miranda, C., et al., *Age-Related Sexual Dimorphism on the Longitudinal Progression of Blood Immune Cells in BALB/cByJ Mice.* The Journals of Gerontology: Series A, 2022. **77**(5): p. 883-891.
49. Earls, R.H., et al., *NK cells clear α-synuclein and the depletion of NK cells exacerbates synuclein pathology in a mouse model of α-synucleinopathy.* Proceedings of the National Academy of Sciences, 2020. **117**(3): p. 1762-1771.
50. Giasson, B.I., et al., *A Hydrophobic Stretch of 12 Amino Acid Residues in the Middle of α-Synuclein Is Essential for Filament Assembly*.* Journal of Biological Chemistry, 2001. **276**(4): p. 2380-2386.
51. Rutherford, N.J., et al., *Studies of lipopolysaccharide effects on the induction of α-synuclein pathology by exogenous fibrils in transgenic mice.* Mol Neurodegener, 2015. **10**: p. 32.
52. Braun, A.A., et al., *Comparison of the elevated plus and elevated zero mazes in treated and untreated male Sprague-Dawley rats: effects of anxiolytic and anxiogenic agents.* Pharmacol Biochem Behav, 2011. **97**(3): p. 406-15.
53. Carpenter, J.M., et al., *Evaluation of delayed LNFPIII treatment initiation protocol on improving long-term behavioral and neuroinflammatory pathology in a mouse model of Gulf War Illness.* Brain Behav Immun Health, 2022. **26**: p. 100553.
54. Krishna, S., et al., *Time-dependent behavioral, neurochemical, and metabolic dysregulation in female C57BL/6 mice caused by chronic high-fat diet intake.* Physiol Behav, 2016. **157**: p. 196-208.
55. Sunyer, B., et al., *Barnes maze, a useful task to assess spatial reference memory in the mice.* protocols.io, 2007.

Figures and Figure Legends

Figure 1

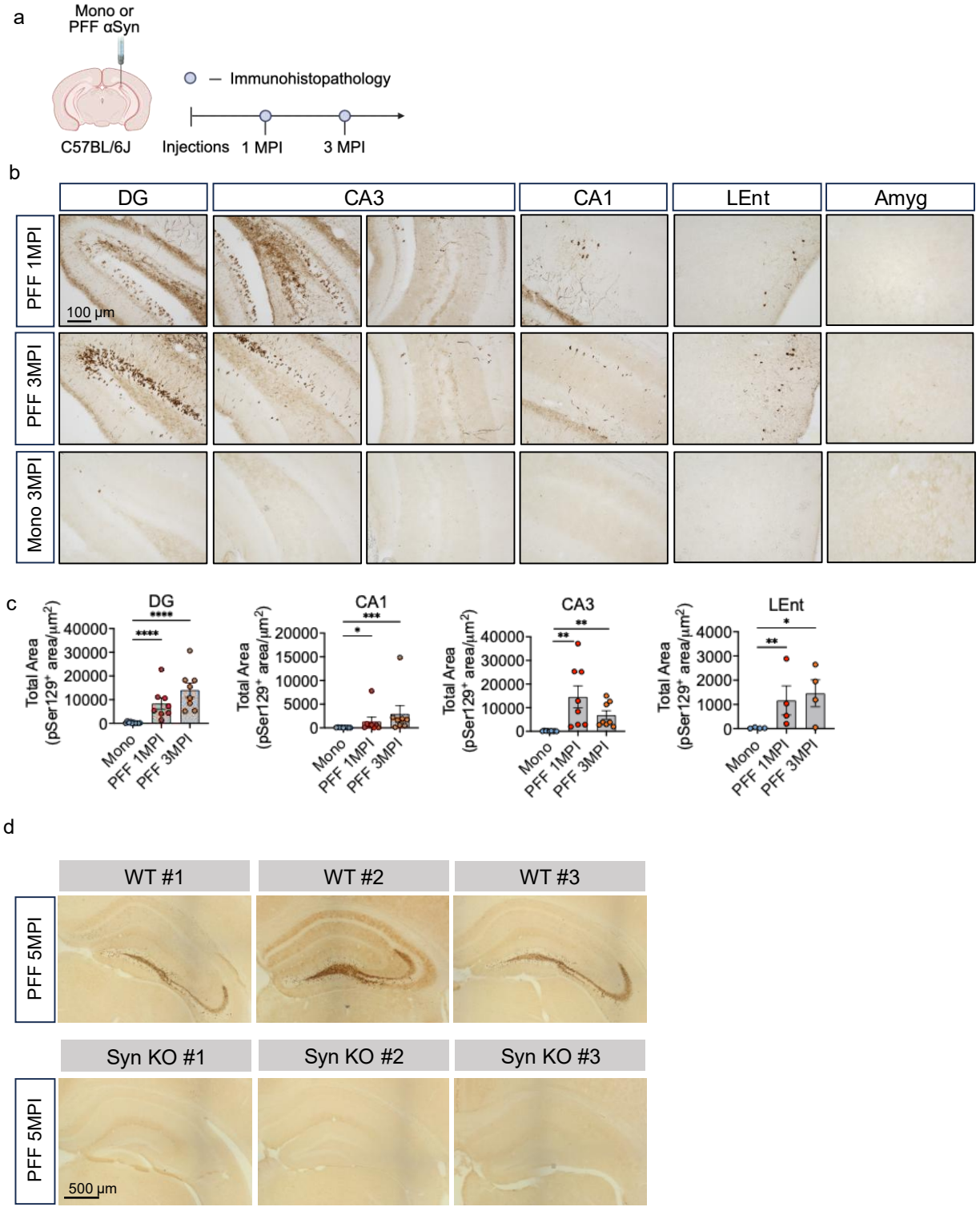


Figure 1. The α-synuclein pathology after PFF α-syn injection in the hippocampus. a) A schematic of the experimental design. Either monomer or PFF αSyn was injected into CA1 and immunohistopathological analyses were performed. **b**) Representative images of the mouse hippocampus subsets (DG, CA1, and CA3), lateral entorhinal cortex (LEnt), and amygdala (Amyg), immunostained with pSer129-αSyn treated with proteinase K at 1- and 3-MPI. Scale bars = 100 μm. c) Graphs represent the average total area of PK-resistant p-α-synuclein+ inclusions per region of interest in the DG, CA1, CA3, and LEnt. Each symbol represents one mouse. Data were pooled from cohorts 1 and 3 for the 3MPI monomer and PFF groups and from cohorts 2 and 3 for the 1MPI PFF group (n=8 per group). Error bars represent ± SEM. Statistical analyses were performed using lognormal Brown-Forsythe and Welch one-way ANOVA, followed by Tukey's multiple comparisons test. $*P < 0.05$, $**P < 0.01$, $***P < 0.001$. **d**) Representative images of the mouse hippocampus of WT and Syn KO treated with proteinase K and immunostained with pSer129 at 5MPI.

Figure 2

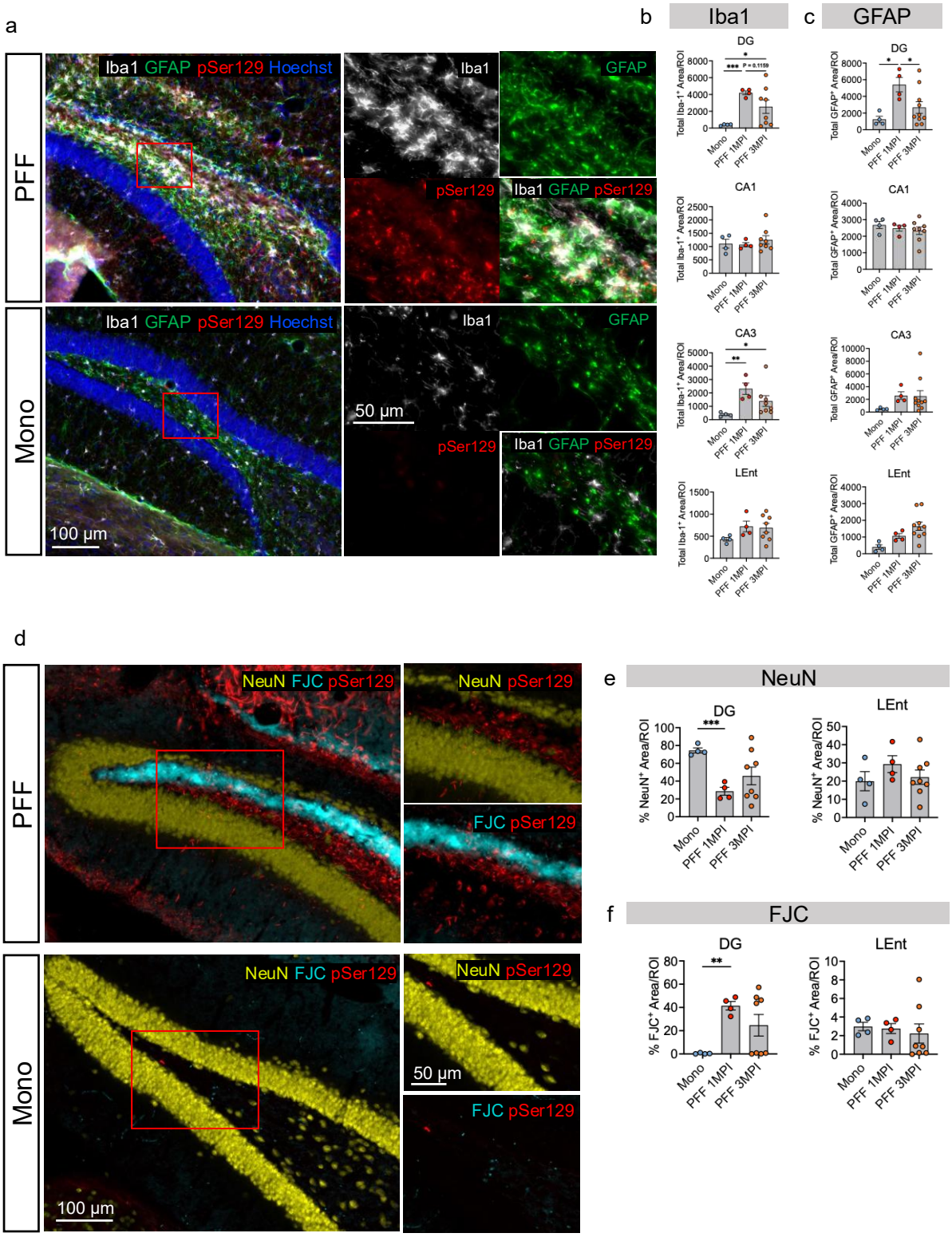

a
b
Iba1
c
GFAP
PFF
Mono
Iba1 GFAP pSer129 Hoechst
Iba1
GFAP
pSer129
Iba1 GFAP pSer129
50 µm
100 µm
DG
CA1
CA3
LEnt
Total Iba-1+ Area/ROI
Total GFAP+ Area/ROI
Mono
PFF 1MPI
PFF 3MPI
d
NeuN FJC pSer129
NeuN pSer129
FJC pSer129
e
NeuN
% NeuN+ Area/ROI
f
FJC
% FJC+ Area/ROI

Figure 2. PFF-induced α-syn pathology drives neuronal degeneration and glial responses in the hippocampus. a) Representative images of the mouse hippocampus (DG) immunostained with Iba-1 (white), GFAP (green), pSer129 (red), and Hoechst (blue) from PFF (1MPI) and Mono (3MPI). Scale bars = 100 µm for 20 X and 50 µm for 100 X. **b**) Graphs represent the total area occupied by Iba-1$^+$ or **c**) GFAP$^+$ inclusion per ROI in the DG, CA1, CA3, and LEnt. Error bars represent ± SEM. Statistical analyses were performed using lognormal Brown-Forsythe and Welch one-way ANOVA, followed by Tukey's multiple comparisons test. *$P < 0.05$, **$P < 0.01$, ***$P < 0.001$. **d**) Representative images of the mouse hippocampus (DG) immunostained with pSer129 (Red), FJC (Cyan), and NeuN (Yellow) of PFF (1MPI) and Mono (3MPI). Scale bars = 100 µm for 20 X images and 50 µm for 50 X images. **e**) Quantification of NeuN$^+$ area (%) or f) FJC$^+$ (%) per ROI in the DG. Each symbol represents one mouse. The 3MPI monomer and 1MPI PFF groups were obtained from cohort 3 (n = 4 per group). The 3MPI PFF group comprised pooled data from cohorts 1 and 3 (n = 8). Error bars represent ±SEM. Statistical analyses were performed using Brown-Forsythe and Welch one-way ANOVA, followed by Dunnett T3 multiple comparisons test. *$P < 0.05$, **$P < 0.01$, ***$P < 0.001$.

Figure 3

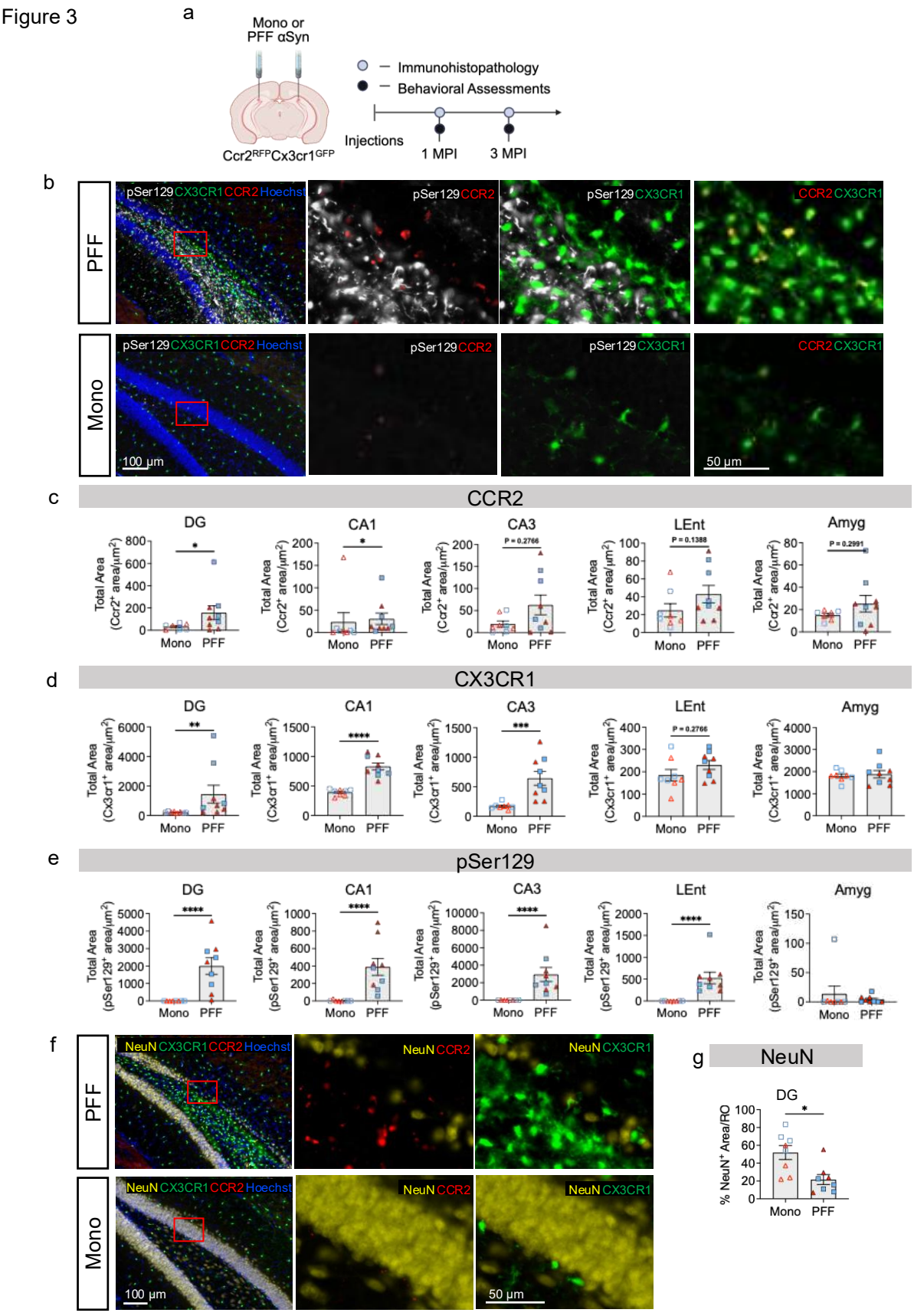

a
Mono or
PFF αSyn
Ccr2RFPCx3cr1GFP
Immunohistopathology
Behavioral Assessments
Injections
1 MPI
3 MPI
b
PFF
Mono
pSer129 CX3CR1 CCR2 Hoechst
pSer129 CCR2
pSer129 CX3CR1
CCR2 CX3CR1
100 µm
50 µm
c
CCR2
d
CX3CR1
e
pSer129
DG
CA1
CA3
LEnt
Amyg
Total Area (Ccr2+ area/µm2)
Total Area (Cx3cr1+ area/µm2)
Total Area (pSer129+ area/µm2)
Mono
PFF
P = 0.2766
P = 0.1388
P = 0.2991
f
NeuN CX3CR1 CCR2 Hoechst
NeuN CCR2
NeuN CX3CR1
g
NeuN
% NeuN+ Area/RC

Figure 3. Hippocampal α-syn pathology, myeloid responses, and neuronal changes following bilateral PFF injection in Cx3cr1^{GFP}/Ccr2^{RFP} mice. a) A schematic of the experimental design. We bilaterally injected either monomeric or PFF αSyn into CA1 and performed behavioral assessments at 1 and 3MPI. **b**) Representative images of the mouse hippocampus (DG) at 1MPI, immunostained with, pSer129 (white), CX3CR1 (green), CCR2 (red), and Hoechst (blue). Scale bars = 100 μm. **c-e**) Quantification of the total area occupied by **c**) CCR2^{RFP}, **d**) CX3CR1^{GFP}, and **e**) pSer129^{+} inclusions per region of interest in the DG, CA1, CA3, LEnt, and Amyg. Error bars represent ± SEM. We performed statistical analyses using the Mann-Whitney U test. *$P < 0.05$, **$P < 0.01$, ***$P < 0.001$, ****$P < 0.0001$. **f**) Representative images of the mouse hippocampus at 1MPI, immunostained with NeuN (yellow), CX3CR1 (green), CCR2 (red), and Hoechst (blue). Scale bars = 100 μm. **g**) Data are presented as mean ± SEM. Statistical comparisons were performed using the Mann-Whitney U test. *$P < 0.05$. Each symbol represents one mouse. At 1MPI, the monomer group comprised 4 males and 4 females (n = 8), and the PFF group comprised 4 males and 5 females (n = 9).

Figure 4

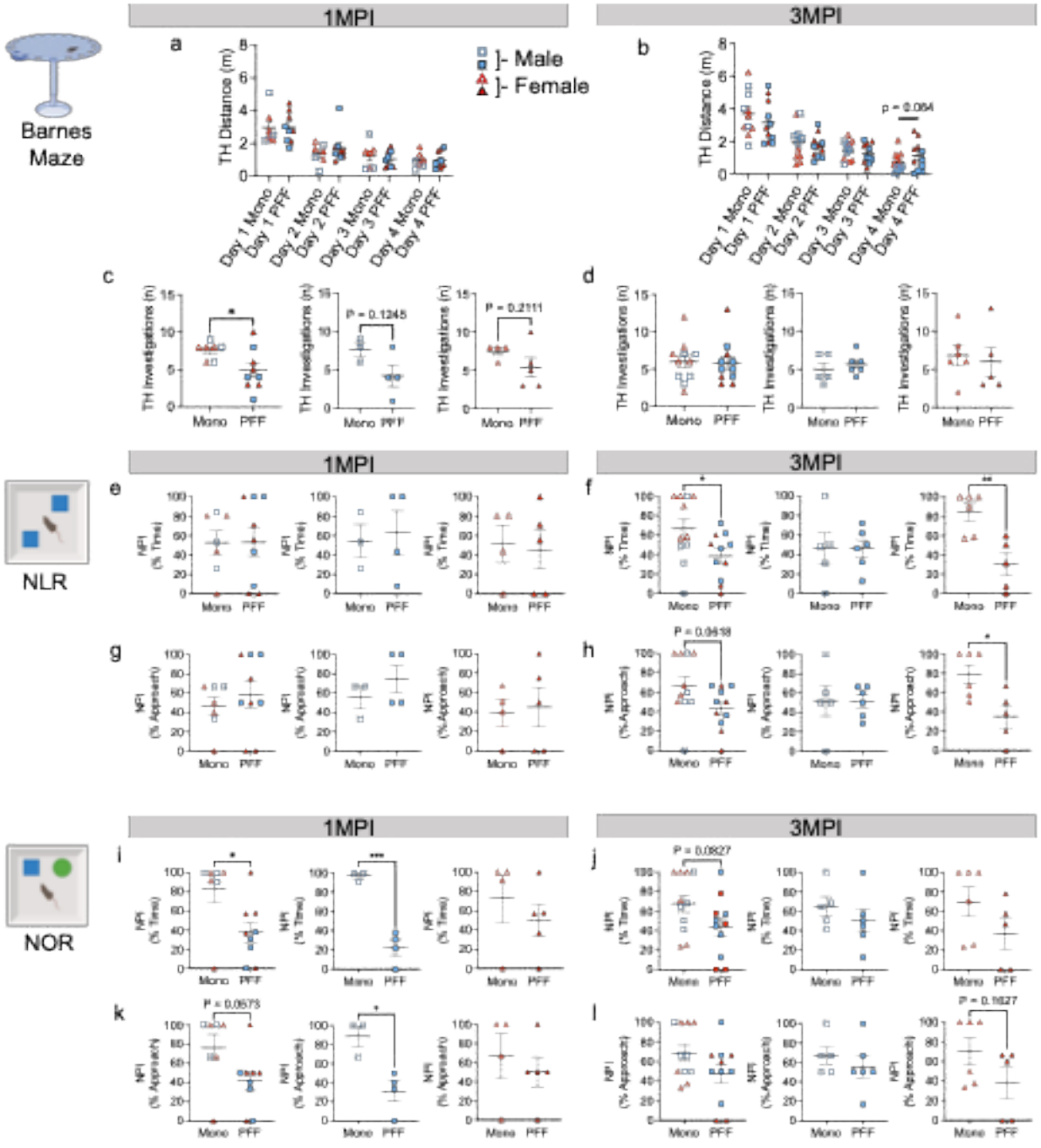


Fig 4. PFF-induced α-syn pathology is associated with selective impairments in spatial and object-recognition memory. a, b) Results from Barnes Maze acquisition at 1MPI and at 3MPI, respectively. **c, d**) Results from Barnes Maze probe trial at 1MPI and at 3MPI, respectively. **e, f**) Novelty preference index (%) by time during the first minute of the NLRT at 1MPI and at 3MPI,

respectively. **g, h**) Novelty preference index (%) by approach during the first minute of the NLRT at 1MPI and at 3MPI, respectively. **i, j**) Novelty preference index (%) by time during the first minute of the NORT at 1MPI and at 3MPI, respectively. **k, l**) Novelty preference index (%) by approach during the first minute of the NORT at 1MPI and at 3MPI, respectively. Each symbol represents one mouse. At 1MPI, the monomer group comprised 3 males and 4 females (n = 7), and the PFF group comprised 4 males and 5 females (n = 9). At 3MPI, the monomer group comprised 5 males and 6 females (n = 11), and the PFF group comprised 6 males and 5 females (n = 11). Error bars represent ± SEM. Barnes maze acquisition data (**a, b**) were analyzed using two-way ANOVA with sex and treatment as factors at each acquisition day. Student-Newman-Keuls pairwise comparisons were used to assess sex differences. On day 4 at 3MPI (**b**), there was a significant main effect of sex ($F(1, 18) = 20.946$, $P < 0.001$), with females traveling farther than males. Neither the main effect of treatment ($P = 0.064$) nor the sex x treatment interaction ($P = 0.319$) was significant on that day. **c-l**) Statistical analyses were performed using an unpaired Student's t-test, $*P < 0.05$, $**P < 0.01$, $***P < 0.001$.

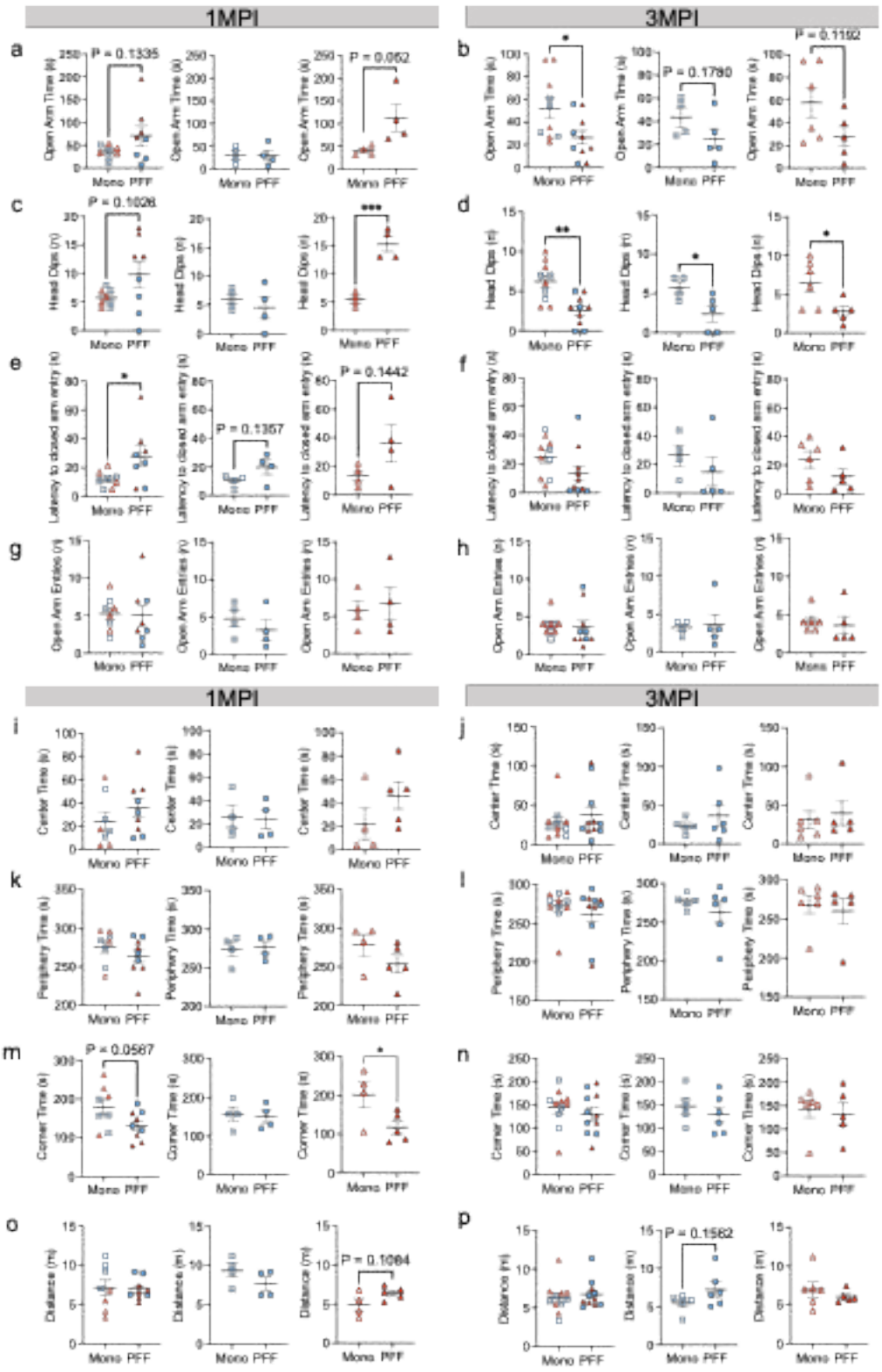
Figure 5



EZM



OFT



898

Fig 5. PFF-induced α-syn pathology is associated with alterations in anxiety-related and risk-assessment behaviors. a, b) Open arm time on the EZM at 1MPI and at 3MPI, respectively. **c, d**) Head dips performed on the EZM at 1MPI and at 3MPI, respectively. **e, f**) Latency to enter the closed arm on the EZM at 1MPI and at 3MPI, respectively. **g, h**) Open arm entries on the EZM at 1MPI and at 3MPI, respectively. **i, j**) Center time during the first 5 minutes of the OFT at 1MPI and at 3MPI, respectively. **k, l**) Periphery time during the first 5 minutes of the OFT at 1MPI and at 3MPI, respectively. **m, n**) Corner time during the first 5 minutes of the OFT at 1MPI and at 3MPI, respectively. **o, p**) Distance traveled during the first 5 minutes of the OFT at 1MPI and at 3MPI. Each symbol represents one mouse. At 1MPI, the monomer group comprised 4 males and 4 females (n = 8), and the PFF group comprised 4 males and 5 females (n = 9). At 3MPI, the monomer group comprised 4 males and 6 females (n = 10), and the PFF group comprised 6 males and 5 females (n = 11). Error bars represent ± SEM. Statistical analyses were performed using an unpaired Student's t-test. $*P < 0.05$, $**P < 0.01$, $***P < 0.001$.

Figure 6

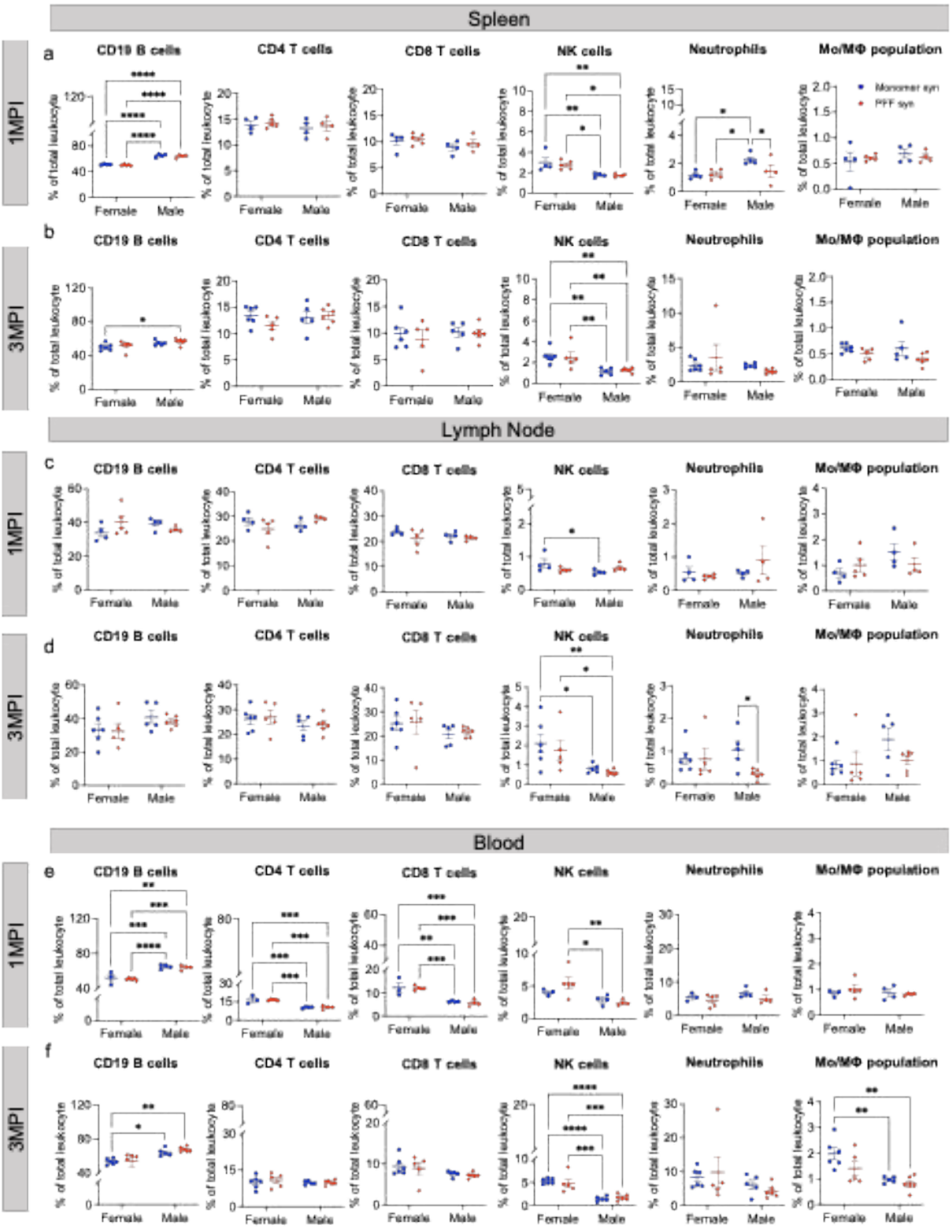

Spleen
Lymph Node
Blood
1MPI
3MPI
a
b
c
d
e
f
CD19 B cells
CD4 T cells
CD8 T cells
NK cells
Neutrophils
Mo/MΦ population
% of total leukocyte
Female
Male
Monomer syn
PFF syn

Fig 6. Hippocampal α-syn PFF injection is associated with reduced peripheral neutrophil frequencies in male mice. Flow cytometric analysis of immune cell frequencies in the **a, b**) spleen, **c, d**) lymph nodes, **e, f**) blood of male and female *Cx3cr1*^{GFP}/*Ccr2*^{RFP} mice following bilateral hippocampal injection of α-syn monomers or PFFs. Samples were collected at **a, c, e**) 1MPI and **b, d, f**) 3MPI. Frequencies of CD19^{+} B cells, CD4^{+} T cells, CD8^{+} T cells, Natural killer (NK) cells, neutrophils, and monocytes/macrophages (Mo/MΦ) are expressed as percentages of total leukocytes. Blue symbols represent monomer-injected mice, and red symbols represent PFF-injected mice. Data are presented as mean ±SEM. Statistical comparisons were performed using two-way ANOVA with treatment and sex as factors, followed by Fisher's LSD test. *$P < 0.05$, **$P < 0.01$, ***$P < 0.001$, ****$P < 0.0001$.

Figure 7

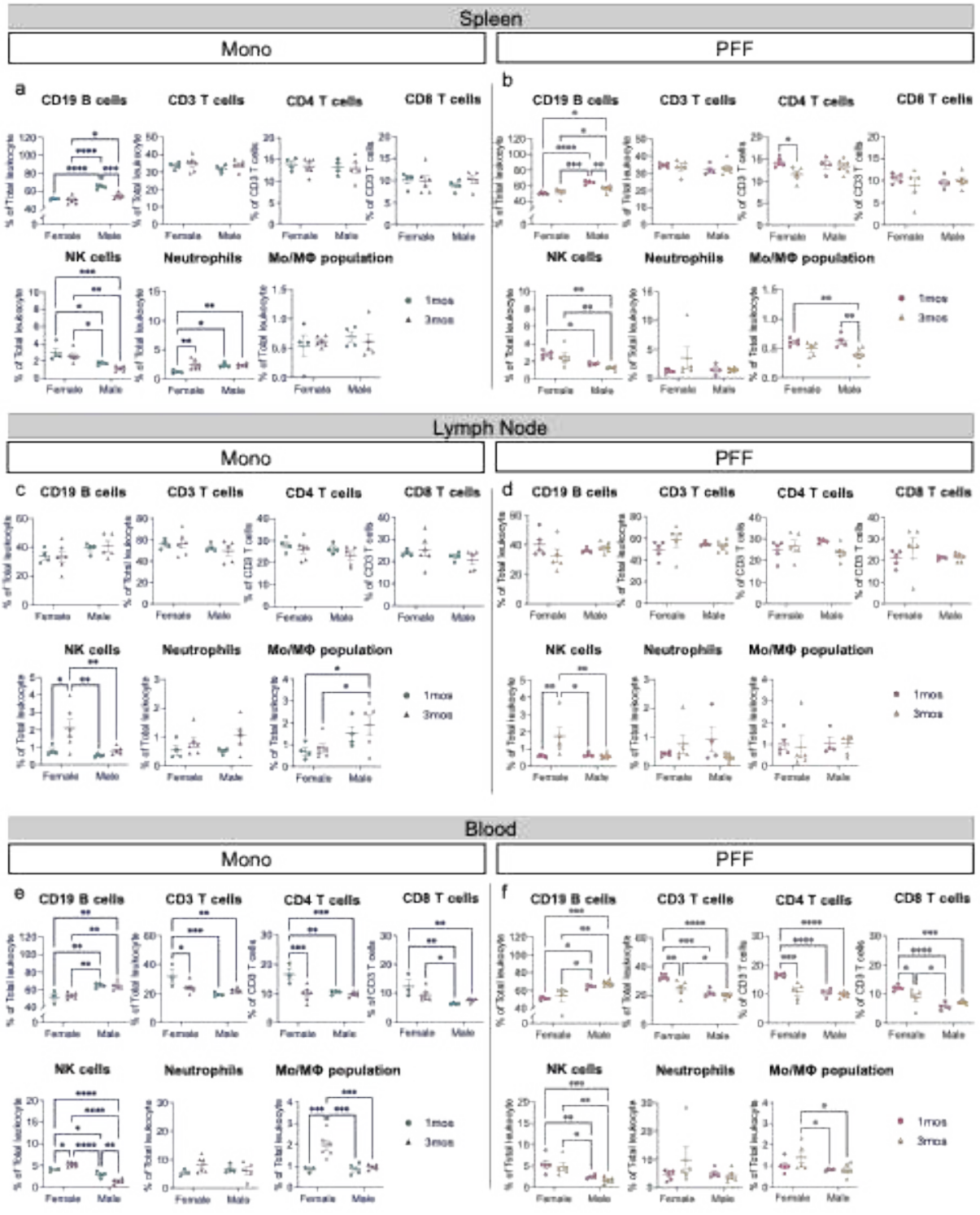


Fig 7. Temporal changes in peripheral immune cell profiles within monomer- and PFF-injected male and female mice. Flow cytometric analysis of immune cell frequencies in the **a, b**)

926 spleen, **c, d**) lymph nodes, **e, f**) blood of male and female *Cx3cr1*^{GFP}/*Ccr2*^{RFP} mice at 1 and 3MPI.
927 Mice received bilateral hippocampal injections of **a, c, e**) α-syn monomers or **b, d, f**) PFFs.
928 Frequencies of CD19^{+} B cells, CD3^{+} T cells, NK cells, neutrophils, and monocytes/macrophages
929 (Mo/MΦ) are expressed as percentages of total leukocytes. CD4^{+} T cell and CD8^{+} T cell
930 frequencies are expressed as percentages of CD3^{+} T cells. In monomer-injected groups, teal circles
931 and purple triangles represent 1 and 3MPI, respectively. In PFF-injected groups, pink circles and
932 orange triangles represent 1 and 3MPI, respectively. Data are presented as mean ± SEM. Statistical
933 comparisons were performed using two-way ANOVA with time and sex as factors, followed by
934 Fisher's LSD test. *$P < 0.05$, **$P < 0.01$, ***$P < 0.001$, ****$P < 0.0001$.

Supplementary Files

This is a list of supplementary files associated with this preprint. Click to download.

- ByunHudsonetalSupplementaryfiguresnpjPD.pdf